Experimental Thermal and Fluid Science xxx (2012) xxx–xxx

Contents lists available at SciVerse ScienceDirect

Experimental Thermal and Fluid Science

journal homepage: www.elsevier.com/locate/etfs

Measurement of heat flux in dense air-mist cooling: Part I – A novel steady-state technique

Constantin A. Hernández-Bocanegra [a,1], A. Humberto Castillejos E. [a,*], Francisco A. Acosta-González [a,1], Xiaoxu Zhou [b,c,1,2], Brian G. Thomas [b,c,2]

[a] Department of Metallurgical Engineering, Centre for Research and Advanced Studies, CINVESTAV - Unidad Saltillo, Carr. Saltillo-Monterrey Km. 13.5, Ramos Arizpe, Coahuila 25900, Mexico
[b] Department of Mechanical Science and Engineering, University of Illinois at Urbana-Champaign, 1206 West Green Street, Urbana, IL 61801, USA
[c] Research & Development Department, SSAB Iowa Inc., 1755 Bill Sharp Blvd., Muscatine, IA 52761, USA

ARTICLE INFO

Article history:
Available online xxxx

Keywords:
Spray cooling
Steady-state method
Boiling heat flux measurement
Dense air mists
Induction heating

ABSTRACT

This work presents a technique for characterizing water air-mist cooling of surfaces at temperatures from 200–1200 °C while subjected to intense spraying conditions, so that the heat flux could reach values in excess of 10 MW/m^2. In this new steady-state method, a local region of an air-mist/spray impinges upon the exposed surface of a hot Pt-disk (8 mm ∅ by 2.5 mm thickness) which is surrounded by an induction coil while both are embedded in a cast ceramic monolith. A digital controller adjusts the output power of a high-frequency generator to balance the induction heating of the Pt-specimen with the heat removed by the boiling of the spray droplets impinging on its active surface, in order to maintain the control temperature of the sample at the predetermined set-point. Measurement of the RMS current flowing through the coil to maintain this temperature, together with the solution of a two-dimensional axi-symmetric computational model of the electromagnetic field and heat conduction equations, enabled estimation of the heat extracted locally by the mist. A rigorous experimental procedure was performed to determine the boiling curves from 200 °C to 1200 °C and then back to 200 °C. The curves for both trajectories revealed that strong boiling hysteresis occurred in the nucleate and transition boiling regimes and that this was almost absent in the stable film boiling regime. On the other hand, hysteresis was not present in thermal loops involving surface temperatures only between 600 and 1200 °C. The existence of hysteresis, in a certain temperature interval, points out the importance of considering the thermal history of actual cooling processes when simulating them in the laboratory. The ability of the new technique to maintain the sample temperature for prolonged periods, e.g., hours, enables future studies to improve the understanding of boiling phenomena during intense heat-removal processes. In Part II of this article, the effects that the mist droplet size, droplet velocity and water impact density have on the heat extracted under steady-state conditions from a surface with large superheat are investigated for a wide variety of those characteristics.

1. Introduction

Spray cooling occurs when a dispersion of fine droplets impacts the surface of a hot body to remove large amounts of heat by vaporization and/or by single phase convection [2,3]. Depending on the system, the surface temperature, T_w, of the body can exceed markedly the saturation temperature, T_s, of the cooling liquid or be slightly above or below it. Hence, any or all of the cooling regimes of a conventional boiling curve [4] can appear. Water-spray cooling technology has found widespread use since it offers a good balance of high heat removal capability, surface temperature uniformity and fluid efficiency. Cases with large surface superheat, i.e., with large T_w–T_s, appear in metallurgical processes (e.g., in continuous casting of steel [5,6] and heat treatment of alloys [7,8]), in safety systems for emergency cooling and pressure control of nuclear reactors [9–11] and in fire suppression/control systems of electrical transformers and flammable material storage tanks [12,13], among many other applications. In more recent times, spray cooling has attracted great interest for the removal of high heat fluxes from surfaces with small superheats, such as the surface of electronic devices [14,15] or human skin [16,17] and from surfaces

* Corresponding author. Tel.: +52 844 438 9600x9666; fax: +52 844 438 9610.
E-mail addresses: constantin.hernandez@cinvestav.edu.mx (C.A. Hernández-Bocanegra), humberto.castillejos@cinvestav.edu.mx (A.H. Castillejos E), andres.acosta@cinvestav.edu.mx (F.A. Acosta-González), xzhou9@uiuc.edu, xiaoxu.zhou@ssab.com (X. Zhou), bgthomas@uiuc.edu (B.G. Thomas).
[1] Tel.: +52 844 438 9600x9666; fax: +52 844 438 9600.
[2] Tel.: +1 217 333 6919; fax: +1 217 244 6534.

0894-1777/$ - see front matter © 2012 Elsevier Inc. All rights reserved.
http://dx.doi.org/10.1016/j.expthermflusci.2012.06.015

Nomenclature

A	operating air flow rate of the nozzle (NL/s)
CHF	critical heat flux (MW/m^2)
ds	differential surface area in electric conductors (m^2)
d_d, d_{30}	drop diameter; volume mean diameter (μm)
f	current frequency (Hz)
Gr	Grashof number, $g\beta\Delta TL3/\nu_o$, in Table 1
h_c, h_{coil}, h_f	heat transfer coefficients: for combined boiling convection plus radiation; for forced convection to the water in the coil tube; for natural convection to the environment surrounding the ceramic body (W/m^2 K)
$\|I\|$, I_m, I_c	magnitude of time-harmonic electric current; measured Root Mean Square (RMS) electric current passing through the coil; computed RMS current (A)
j	imaginary unit number ($=\sqrt{-1}$)
J, $\vec{J}$	magnitude of time-harmonic current density; current density vector (A/m^2)
k_{Pt}, k_{Cu}, k_c	thermal conductivities of Pt; coil; and ceramic (W/mK)
l, r	letters denoting temperature lowering, rising paths in a sample thermal loop
L	length of discretized closed circuit (m)
M	mutual inductance (H)
N	direction normal to the internal surface of the coil tube
Nu	Nusselt number hD/k, in Table 1
p_a, p_w	manometric air inlet; water inlet pressures (k Pa)
Pr	Prandtl number, in Table 1
$-q$, $-q_c$	boiling convection heat flux; combined boiling convection plus radiation heat flux from exposed surface (MW/m^2)
Q_v	heat source resulting from induced current density (W/m^3)
$r_{i,k}$	separation distance between differential length elements of circuits i and k in conductors, (m)
r, z	axi-symmetrical coordinates measured from the metallic disk center in Fig. 2 (m)
Re	Reynolds number in Table 1
S	total cross section area for current flow in each conductor (m^2)
T, T_c, T_m	temperature; computed control; measured control temperatures (°C)
T_L, T_s, T_w, T_∞, T_f	Leidenfrost; saturation; surface; surrounding of sample active surface; surrounding of ceramic body temperatures (°C)
u_{zs}, $u_{z,v}$	drop velocity; normal volume weighted mean velocity (m/s)
V	external voltage applied to a closed circuit (V)
w	local water impact density (L/m^2 s)
W	operating water flow rate of the nozzle (L/s)
x, y, z	rectangular coordinates with origin at center of nozzle orifice (m)
x_i	independent variables in Table 2

Greek

δ	skin depth (m)
δx_i	measurement error of independent variable x_i
ε	emissivity
μ, μ_R	absolute (H/m); relative, μ/μ_o, magnetic permeabilities
μ_o	magnetic permeability of free space, $4\pi \times 10^{-7}$ (H/m)
π	constant, 3.14159264...
ρ	density (kg/m^3)
σ, σ_r	electric conductivity (mho/m); Stefan–Boltzmann constant, 5.669×10^{-8} (W/m^2 K^4)
ω	current frequency, $2\pi f$ (radians/s)

Subindex

i	integer denoting a discretized current circuit
I, R	imaginary; real parts of a complex number
k	integer denoting a discretized electric circuit within a conductor
ϕ	angular direction in cylindrical coordinates

with negative superheat [15,18]. The wide scope of applications entails a huge spectrum of the values of the parameters and properties affecting heat transfer in boiling and this has demanded the development and use of good experimental methods for studying the governing mechanisms of this very complex process.

The heat transfer performance of droplet streams, water sprays and air-mists has been experimentally investigated using both steady- and unsteady-state methods. In the steady-state methods, a specimen is heated by a thermal power source, Q_v, while simultaneously being spray cooled to remove a heat flux, $-q$, to maintain a constant temperature distribution throughout [3,15,19–35]. Hence, the surface temperature, T_w, and the associated heat transfer coefficient, h, are evaluated using Fourieŕs law of heat conduction and Newton's law of convection. On the other hand, the transient methods are based on exposing the surface of a hot test-specimen to the spray and simultaneously recording its temperature–time history at specific locations near its surface while it cools [16,17,25,28,34–41]. Estimation of T_w and h requires the numerical calculation of the transient heat flux, through the solution of an inverse heat conduction problem. From the literature, it is clear that transient methods allow measurements over all of the different regimes of the conventional boiling curve, i.e., stable film boiling, transition boiling, nucleate boiling and single phase convection, across broad ranges of T_w and under low and high water impact density, w, values. On the other hand, the reported steady-state experimental tests have been mostly restricted to temperatures in the single phase convection regime [3,15,18], the lower part of the nucleate boiling regime [29–31] and to very narrow temperature intervals in the film boiling regime [21,23,25,27,29,30,33], i.e., to low temperatures and to regions where the boiling heat flux varies little with temperature. Fewer studies have included the transition boiling regime where the heat flux varies appreciably with T_w. These last studies have involved streams with low droplet frequencies [19,20] and sprays with w in general smaller than 5 L/m^2 s and T_w less than 500 °C [22,26,32,34].

Only a few comparisons between steady and unsteady procedures have been reported. In a study involving a plane water jet impinging on a hot surface, Ishigai et al. [23] found that in the nucleate boiling regime the two methods led to different heat fluxes and the discrepancy was attributed to inaccuracies in their unsteady method, while in the film boiling regime both techniques matched reasonably well. Olden et al. [34] found that the two methods compared well in the transition regime for $w = 2$ L/m^2 s and temperatures within 200–500 °C, but not in the nucleate boiling regime. However, the comparison did not involve strictly similar spraying conditions. Investigators have reported pros and cons of both methods. Thus, it has been claimed [33] that steady methods are more convenient for determining the dependence of h on nozzle operating conditions in the film boiling regime, and that transient techniques are better suited for studying the dependence of h with T_w, particularly in the transition boiling regime. Also, it has been argued that steady-state methods are faster than unsteady ones [27,33] and additionally, that they have the inherent advantage of being independent of the response time of the thermocouples and

Please cite this article in press as: C.A. Hernández-Bocanegra et al., Measurement of heat flux in dense air-mist cooling: Part I – A novel steady-state technique, Exp. Therm. Fluid Sci. (2012), http://dx.doi.org/10.1016/j.expthermflusci.2012.06.015

the data acquisition system [33]; the first assertion however was not substantiated. The application of steady-state methods has been limited by the maximum attainable power densities, which restrains the size of the test-specimen, the water impact flux that can impinge upon it, the maximum specimen temperature and the time that the steady-state can be maintained. Schmidt and Boye [30] reported a steady-state apparatus where T_w could be held constant for a period of 10–60 s at $w \leqslant 2.5$ L/m^2 s. Ciofalo et al. [37,38] claimed that for samples with cross section areas of 0.04×0.05 and 0.075×0.075 m^2 and a few millimeters thickness, the electric powers required to keep them at constant temperature would be prohibitive if the probes (i.e., if the devices designed to investigate the heat transfer) were subjected to a heat flux extraction of 10 MW/m^2. Furthermore, the investigators [37,38] indicated that a control system would be unable to maintain steady-state conditions in the transition boiling regime. The measuring apparatus of Olden et al. [34], which used a flame burner as the heating source, was confined to temperatures between 70 and 500 °C and to a maximum w of 2 L/m^2 s when operating in steady mode, but it did not have these limitations in transient mode.

In past literature, different types of heating sources have been used to investigate boiling heat transfer coefficients with sprays. In steady-state test rigs, the type of heating source is critical since it must provide sufficient power to balance the heat extracted by the spray through the active surface(s) of the body plus the heat lost through the other faces. Also, the heating device must neither interfere with the spray, nor cause hazardous conditions and should be able to undergo automatic control. Heating methods have involved direct resistance heating [3,20,23,25,27,30,32], electrical resistance cartridges, bands or plates [15,18,19,21,22,24,26,31] and gas burners [29,33–35]. Direct electrical resistance heating involves passing current through a thin test-plate to heat it by the Ohmic resistance of the test material itself. The same Ohmic effect heats up the electrical-resistance elements, which in turn are mounted in watertight intimate contact with the test-specimen to heat it by conduction. Direct resistance heating methods have been applied for $2.5 \leqslant w$ (L/m^2 s) $\leqslant 33.3$ and over a narrow range of surface temperatures in the film boiling regime, 900–1000 °C [25,27]. Toda [22] used electrical heating elements to study the air-mist cooling of a metallic surface, at up to 300 °C, while subjected to a water flux in the range of $3.4 \leqslant w$ (L/m^2 s) $\leqslant 14.3$. Other works employing electrical rod elements have studied mist cooling of surfaces at temperatures below the normal boiling point of the cooling liquid [15,18] or of surfaces held between 200 and 900 °C while impinged by streams of drops with a frequency of 0.5–3.0 drops/s [20]. Jenkins et al. [33] studied air-mist cooling of a surface at 800 °C with water-fluxes between 0.51 and 16 L/m^2 s, employing a gas flame as the heating source. The use of induction heating in steady-state apparatuses, to measure boiling heat transfer coefficients with sprays, has not yet found application. It has been claimed that the coil wrapped around the test-specimen would interfere with the flow of water from the spray [29]. The advantages of induction heating have been exploited in a transient technique [38].

The maximum heat fluxes measured by steady-state methods have been a fraction [18,29,32] or at most a few MW/m^2 [3,19,21,22,26,31]. Mudawar and Valentine [26] reported critical heat fluxes close to 6 MW/m^2, at 122 °C, for water spraying conditions involving $w = 5$ L/m^2 s and drops with mass median diameters and average velocities between 763 and 1872 μm and 11.7–18.1 m/s, respectively.

From the classic pool boiling investigation carried out by Nukiyama [42], the type of control, i.e., power or temperature control, used in steady-state heat flux measuring methods has been found to affect the form of the typical boiling curve. Methods that control the power supplied to the hot body leave the surface temperature to vary as the dependent variable, while in methods which control the temperature, the power is dependent. Commonly, it is believed that in steady-state experiments under temperature control, the heat-flux variation with surface superheat ΔT is univocal; i.e., for a given ΔT, the heat $-q$ extracted from the surface reaches a unique equilibrium power [43,44]. As T_w rises above T_s, the heat flux $-q$ increases along the single phase convection and nucleate boiling regimes until reaching a maximum critical heat flux, CHF. Further increase in T_w leads to a decrease in $-q$ along the transition boiling regime until reaching a minimum at the Leidenfrost temperature, T_L. Above this temperature, $-q$ increases again in the film boiling regime. From high to low temperatures – with temperature control – the evolution of $-q$ with ΔT was foretold by Nukiyama [42] to simply reverse its path along the same boiling regimes. This behavior has been later found in some works involving low boiling point organic liquids [45,46]. Differently from this behavior, with power control, increasing the power to above CHF causes the transition boiling regime and the lower portion (with $-q \leqslant$ CHF) of the stable film boiling regime to be bypassed due to an abrupt increase in surface temperature, that equilibrates the power supplied with a corresponding film-boiling heat flux greater than CHF. Returning from high to low power – with power control – the film boiling regime of the classic curve will be followed. Then, upon reaching T_L, further decrease in power will cause an abrupt drop in surface temperature bypassing the transition boiling regime and the portion of the nucleate boiling regime with surface heat flux above the value corresponding to T_L [42]. The departure from the classical boiling curve appearing at the burnout (during heating) and Leidenfrost (during cooling) points constitutes a hysteresis type that intrinsically accompanies the power-controlled methods. In addition, nucleation hysteresis and several other types of hysteresis have been reported for liquid jet [47] and pool [48] boiling systems operating under power control. Hysteresis becomes more pronounced in systems involving highly wetting liquids and porous surfaces.

It has been found that even in temperature controlled systems, boiling hysteresis may be present. The analysis of Witte and Lienhard [49] of pool-boiling heat-flux measurements with organic liquids [50,51] supports the idea of a non-univocal relationship between $-q$ and ΔT, while passing through the transition boiling regime following increasing and decreasing temperature paths. Rajab and Winterton [52] carried out steady- and unsteady-state experiments using deionized water and an organic liquid. In their steady-state tests with both temperature-rising and temperature-lowering paths, the nucleate boiling, film boiling and most of the transition boiling regimes were present. Although the curves from both paths overlapped in the nucleate and film boiling regimes, the determined part of the curves corresponding to transition boiling regime differed, revealing hysteresis in agreement with Witte and Lienhard [49]. The heat flux at a given ΔT during temperature rising was higher than that measured along the temperature lowering path. The independent measurement of solid–liquid contact indicated that liquid–surface interaction was higher on heating than on cooling in the temperature range of transition boiling, thus explaining the higher values of $-q$ obtained during the heating path [52]. The contradictory findings revealing the non-existence [45,46] and existence [49,52] of different transition boiling curves for heating and cooling paths indicate that further study of boiling is needed [53], even in pool boiling systems that have been studied more than spray cooling.

From this literature review, it is clear that previous experimental investigations using steady-state methods have studied spray conditions involving moderate heat fluxes and low surface temperatures (<500 °C) or a narrow range of higher temperatures. The most commonly reported spray characteristic is water impact flux, w, which has been usually smaller than 5 L/m^2 s. In contrast to these conditions, the secondary cooling of continuously cast steel, which is the motivation behind this work, involves surface

Please cite this article in press as: C.A. Hernández-Bocanegra et al., Measurement of heat flux in dense air-mist cooling: Part I – A novel steady-state technique, Exp. Therm. Fluid Sci. (2012), http://dx.doi.org/10.1016/j.expthermflusci.2012.06.015

temperatures and water impact densities that are considerably higher. The surface temperatures typically range from 1200 to 750 °C, and for practical nozzle operating conditions, w typically varies from 10–90 L/m^2 s, over a large fraction of the mist footprint areas. These conditions have been appropriately handled by a transient heat-flux measuring method, to obtain heat transfer correlations [5,41] to mathematically model the cooling and solidification of thin steel slabs [5,54,55]. However, with the transient free cooling technique, the cooling of the test-specimen occurs so fast that it is difficult to observe the boiling phenomena, and it is impossible to study time-related effects such as hysteresis or the formation of surface deposits on heat extraction. Therefore, as a first step towards investigating these aspects of spray cooling, this work presents a novel steady-state technique based on balancing the heat extracted from the sample surface by the boiling water droplets, with the heat supplied by electromagnetic induction. In this technique, the measurement of the RMS current, I_m, flowing through the coil to maintain a desired sample temperature, T_m, together with the solution of a two-dimensional axi-symmetric computational model of the electromagnetic field and heat conduction equations has enabled estimation of the heat extracted by spray cooling. The technique falls in the category of temperature controlled techniques [43,44,53] and our results indicate that the steady-state technique presented here enables the precise and systematic measurement of entire boiling curves under the intense spraying conditions used in processes involving surfaces with large superheat.

2. Experimental techniques

2.1. Test rig and conditions

As indicated above, the steady-state measuring method developed here to quantify boiling heat transfer is based on equalizing the induction heating of a metallic sample with the heat removed by the boiling of spray droplets that impinge upon the uncovered surface of the test-sample. To accomplish these measurements, the following equipment was used: (a) a generator with enough output power to compensate the sample heat losses; (b) a coil with the required design and shape near the surface of the specimen to ensure its fast heating; (c) a digital controller to maintain the specimen at the desired set-point temperature; (d) water and air supply systems capable of delivering constant flow rates to the nozzle and to maintain steady spraying of the sample; (e) a traversing mechanism for moving the nozzle and exposing the specimen to different locations of the spray cross-section and hence to different water impact densities, droplet diameters and droplet velocities; and (f) an acquisition and computer system for data logging and data processing. Fig. 1 shows the test rig made-up of all these components.

The high frequency 50–450 kHz generator (Luzars URF-5, ASEPSA S.A. de C.V., QRO, Mexico) had a nominal output power of 5 kW, and a maximum RMS output current of 60 A. The generator included a port for external control through the application of a voltage input in the range of 0–5 VDC, for 100% of the output power range. A PID (proportional–differential–integral) digital controller (A5AK-AA2-500, Omron Corp., Kyoto, Japan) provided this input voltage. The controller measured the temperature of the thermocouple welded in the back face of the sample and compared it to the specified set-point value. Based on their difference and the defined PID gains, the controller adjusted the voltage to provide the required output power of the generator. Additionally, the generator was instrumented with a high frequency ammeter (TRC-4000, ASEPSA S.A. de C.V., QRO, Mexico) designed and built for the specific coil configuration. Basically, this ammeter is a current transformer that measures the AC RMS current passing through the coil by converting it to a proportional DC output signal. The AC current can be up to 1000 A at 400 kHz and is transformed to DC signals in the ranges of 0–10 V, 0–20 mA, or 4–20 mA. The ammeter circuit was calibrated by applying known AC signals and measuring the DC output current. The error limits of the ammeter were ±0.8% at 200–500 A and 250 ± 10 kHz, which include the current and frequency intervals found in the present experiments.

Water for the air-mist nozzle was supplied from a reservoir using an immersion pump and the line was instrumented with a digital turbine flow-meter, a valve, a digital pressure gauge and an immersion thermocouple. For the experiments, well water was softened to minimize the deposition of a crust of calcium and magnesium sulfates on the surface of the Pt-specimen. After treatment, the concentrations of the main ions in the water were as follows: $Ca^{2+} < 0.25$ mg/L, $Mg^{2+} \sim 50$ mg/L and $Na^{+} \sim 600$ mg/L. The air was provided by a compressor and the line included an automatically controlled valve, to minimize flow rate variations, a mass flow-meter and a digital manometer. The capacity of both lines could handle the flow specifications of a wide variety of spray and air-mist nozzles used for secondary cooling in the continuous casting of steel. Selection of the x–y–z position of the Pt- specimen with respect to the center of the nozzle orifice was achieved via a traversing mechanism on which the nozzle was mounted. The nozzle orifice was held at a specified setback distance, z_s, from the surface of the platinum disk, and the transverse x-position varied at $y = 0$; as shown in the coordinate system in Fig. 1, the origin is located at the center of the nozzle orifice. As appreciated from the figure the nozzles were of the fan discharge type. Part II of this work reports the setback distance, the angle of expansion of the fan jets, and the relationship between the flow rates (W and A) and operating pressures (p_w and p_a) of the water and air in the pneumatic nozzles [1]. The nozzles investigated were: W19822 (Delavan Inc., Monroe, NC), Casterjet 1/2–5–60 and Casterjet 1/2–6.5–90 (Spraying Systems Co. Chicago, IL), but this article (Part I) presents representative results only for W19822 nozzles. Data acquisition was accomplished by a SCXI-1000-NI system driven by LabView (National Instruments Corp., Austin, TX). The data sampled by the system were: the output power of the generator, the coil RMS current and current frequency, the specimen control temperature, the water temperatures at the entrance and exit of the coil, the temperature of the water fed to the nozzle and the water and air flow rates and pressures in the nozzle. The water temperature was measured with K-type thermocouples.

2.2. Measuring probe

The test specimen shown in Fig. 1 consisted of a platinum disk (8 mm ∅, 2.5 mm thickness) instrumented with an R-type thermocouple (0.5 mm ∅) that was welded to the center of its back surface. This specimen was wrapped around by a hollow copper coil, and all were encased in insulating SiO_2 castable ceramic to form a monolith. Care was taken to ensure that, in its as-cast state, the ceramic completely filled the gaps between the specimen and the coil and established an intimate union with both of them, leaving no crevices in between. As seen in the figure, the monolith was placed inside a Plexiglas tube and its front was covered by a quartz window having a central hole. This probe or test-assembly left only the frontal face of the Pt-disk exposed to the impingement of the spray water droplets.

The thermocouple at the back of the disk registered what is called the sample or control temperature T_m. As shown in Fig. 1, the terminals of the coil exited through holes in the Plexiglas tube and the thermocouple was withdrawn through a small orifice on the back cover. For additional protection against water, the ceramic body was coated with waterproof paint. As shown in the figure, the coil had two turns and was formed in a mold that flattened a

Please cite this article in press as: C.A. Hernández-Bocanegra et al., Measurement of heat flux in dense air-mist cooling: Part I – A novel steady-state technique, Exp. Therm. Fluid Sci. (2012), http://dx.doi.org/10.1016/j.expthermflusci.2012.06.015

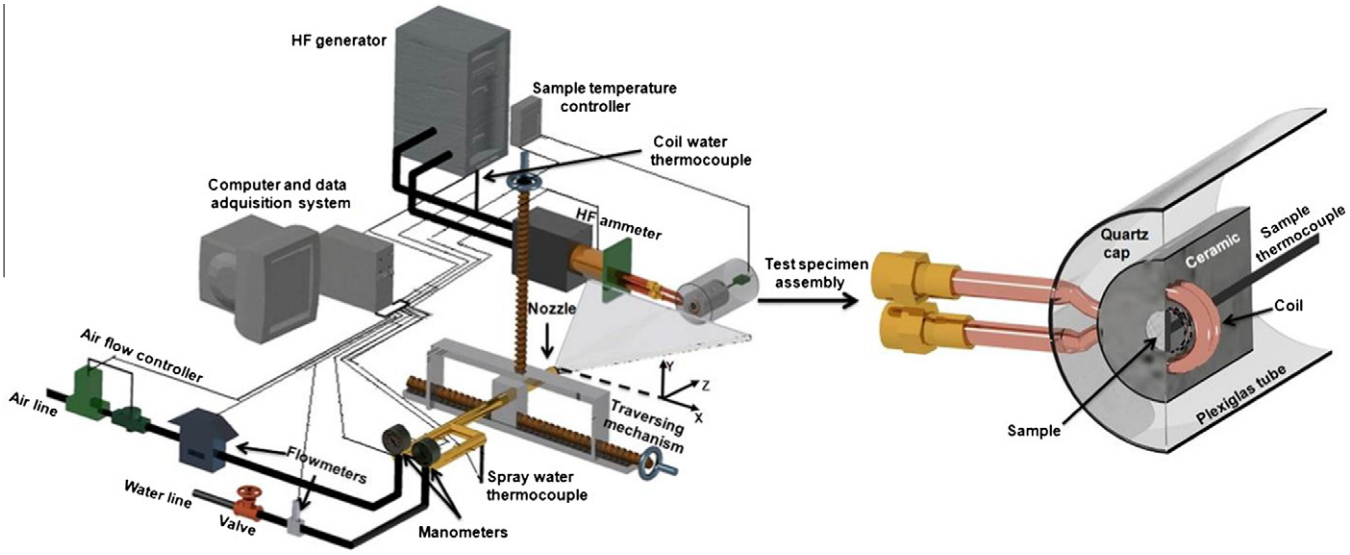

Fig. 1. Schematic of experimental facility.

copper-tube of 3.175 mm internal diameter. The forming procedure allowed closing the turns tightly, i.e., allowed to complete each of the turns as completely as possible and to minimize variations among fabricated coils, in spite of the small coil diameter. The platinum disk exhibited excellent dimensional stability and did not present any noticeable oxidation under the test conditions employed. These characteristics ensured the maintenance of a constant separation between the specimen and the coil, favoring stable induction and a tight sealing of the lateral disk face by the ceramic, which thereby inhibited water penetration. During construction of the test-assembly, a centering device was used to align the center of the disk with the center of the coil, before the ceramic was cast. The quartz window had a thickness of only 0.5 mm, so it did not form a thick step for the accumulation of water, and also did not produce any significant shadow that could interfere with the arrival of droplets to the front of the platinum disk, for those tests which were off-center relative to the nozzle axis. The thermo-physical properties of the components of the test-assembly are listed in Table 1 and their typical dimensions are displayed in Fig. 2. However, as noticed in Section 2.5 small variations in the dimensions of certain probe components have an important influence on the measured heat flux, so all dimensions were measured for each individual assembly. Also, since the manufacturing of the test-assembly affects the conductivity of the ceramic body (possibly by differences in the resulting porosity) this thermal conductivity was determined for each probe according to the procedure described in Section 2.4.

In the mist cooling experiments reported here, the control temperature in the sample was varied in stepwise gradations of 100 °C, first increasing and then decreasing. Two thermal loops were studied: 200–1200–200 °C and 600–1200–600 °C, as well as, a temperature path from 1200 to 600 °C. At each step, the control temperature was held for ~480 s, which was sufficient time for the control temperature of the sample and the RMS current in the coil to reach steady values. As seen in Section 2.3, the determination of the heat flux lost by the sample through its exposed surface was based on these steady-state values.

2.3. Analysis of the experimental data

During each spray-cooling experiment, thermal equilibrium of the test-assembly was defined when the measured temperature, T_m, at the center of the back surface of the Pt-sample became equal to the set-point, specified in the controller, and the measured RMS (i.e., root mean square) current, I_m, passing through the coil stabilized at a particular value, such that the heat input by electrical energy compensated exactly the heat losses through its boundaries. Additionally, considering that each coil turn closely approximates a toroid, axial symmetry of the test-assembly can be assumed, as shown in Fig. 2. Therefore, the energy balance in this domain can be written as the steady 2-D axi-symmetric heat conduction equation,

$$\frac{1}{r}\frac{\partial}{\partial r}\left(rk\frac{\partial T}{\partial r}\right)+\frac{\partial}{\partial z}\left(k\frac{\partial T}{\partial z}\right)+Q_v=0 \tag{1}$$

where r and z are radial and axial coordinate positions, k and T are thermal conductivity and temperature and Q_v is a source term representing the generation of power per unit volume. The last term arises from the Joule resistance heating effect associated both with the flow of total current through the Cu-coil and with the current induced electromagnetically. The induced current heats the Pt-specimen and the coil current generates heat that also affects the thermal state of the probe. The source term Q_v can be expressed as,

$$Q_v=\frac{1}{2\sigma}\mathrm{Re}\{\vec{J}\cdot\vec{J}\}=\frac{1}{2\sigma}\mathrm{Re}\{J^2\} \tag{2}$$

where σ is the electrical conductivity of the particular conductor, i.e., Pt or Cu, and Re stands for the real part of the square of the modulus of the current density, $\vec{J}$, passing through each of them. Fig. 2 shows the boundary conditions for this heat conduction problem: (a) symmetry at the axis; (b) free convection to the ambient air through the back and lateral surfaces; (c) forced convection from the internal walls of the coil to the water flowing inside; (d) zero heat flux through the quartz cap, because the air gap between it and the front surface of the ceramic prevents significant heat losses from this surface; and (e) combined heat flux losses from the front face of the Pt-disk, $-q_c$, consisting of boiling convection, $-q$, plus radiation given as,

$$-q_c=-q+\sigma_r\varepsilon(T_w^4-T_\infty^4)=h_c(T_w-T_\infty) \tag{3}$$

where σ_r is the Stefan–Boltzmann constant ($=5.669\times10^{-8}$ W/m^2 K^4), ε is the emissivity of Pt defined in Table 1 and T_∞ and T_w are the ambient and surface temperatures in degrees Kelvin, respectively. To estimate the unknown boiling convection heat flux, $-q$, requires solving the inverse heat conduction problem for the combined heat transfer coefficient, h_c, by minimizing the error between

Table 1
Thermo-physical properties and heat transfer parameters.

Material	Thermal conductivity k (W/mK)	Emissivity (ε)	Density ρ (kg/m^3)	Electrical conductivity σ (mho/m)	Relative magnetic permeability,[a] (μ_R)
Thermophysical properties of test-assembly materials					
Platinum	$71.3382 + 2.2147 \times 10^{-3}T + 1.0035 \times 10^{-5}T^2$[b]	$0.031555 + 1.3972 \times 10^{-4}T - 2.1119 \times 10^{-8}T^2$[b]	21450	$[1.75 \times 10^{-8}$ $1 + 0.0039(T - 20)]^{-1}$[b]	1
Copper (at 100 °C)	390	–	8900	4.3×10^7[c]	1
Ceramic	0.58[d]	–	1762	–	–
Heat transfer coefficients					
Natural convection to air h_{air}		W/m^2 K	10; from correlation Nu = 0.54 $(GrPr)^{0.25}$[e]		
Forced convection to cooling h_{Cu}		W/m^2 K	55470; from correlation Nu = 0.023 $Re^{0.8}Pr^{0.4}$[e]		

[a] $\mu R = \mu/\mu_o$, where μ is the magnetic permeability and μ_o ($= 4\pi \times 10^{-7}$ H/m) is the free space magnetic permeability.
[b,c,d,e] Obtained from Refs. [56–59], respectively.

the computed, T_c, and the measured (control), T_m, sample temperatures. The h_c and $-q$ values obtained represent average values over the surface of the sample and their estimation requires solving for the current density distribution, $\vec{J}$, in the sample and in the coil to evaluate Q_v according to Eq. (2).

In AC circuits, the electric current concentrates mainly in the periphery of the conductor [60], in the so called skin-depth which for a uniform plane wave has a thickness, δ, given as,

$$\delta = \frac{1}{\sqrt{\pi f \mu \sigma}} \tag{4}$$

where f is the current frequency, μ is the magnetic permeability and σ is the electrical conductivity. Hence, the current density appearing in Eq. (2) varies substantially through the cross-section area of the conductors. For axi-symmetric configurations, as the present one, the current density has a nonzero component only in the angular direction, φ, which is given as,

$$J_\phi = J_{\phi,R} + jJ_{\phi,I} \tag{5}$$

where the subscripts R and I denote the real and imaginary parts of the time-harmonic angular current density, J_ϕ, and $j = \sqrt{-1}$. The magnitude of the total current, $|I|$, passing through the conductors can be calculated by integrating J_ϕ over their cross section area, S, and taking the norm according to,

$$|I| = \sqrt{\left(\int_S J_{\phi,R} ds\right)^2 + \left(\int_S J_{\phi,I} ds\right)^2} \tag{6}$$

from which the total RMS current $I_{RMS}(= |I|/\sqrt{2})$ can be computed; this quantity was measured by the high frequency ammeter mentioned in Section 2.1. Hence, Q_v can be estimated by computing the current density distribution associated with the measured RMS current, I_m. This can be done using the mutual inductance method [61], MIM, which expresses that,

$$\frac{J_k L_k}{\sigma_k} + j\omega \int_S J_i M_{i,k} ds = V_k \tag{7}$$

for conductors subjected to a high frequency electromagnetic field in an axi-symmetric domain. The MIM equation relates the Ohmic voltage and the induced electromotive force, terms on the left, to the external voltage applied to an AC circuit, term on the right. In the equation, the subscript k (= 1, 2,…i,…,n) denotes discrete closed circuits of differential cross section area ds and length L_k, shaping-up the conductors in the system with a total surface area S; ω (= $2\pi f$) is the current frequency (s^{-1}); V_k is the external voltage applied to a closed circuit of length L_k and $M_{i,k}$, which is a measure of the inductive interaction between closed circuits i and k, is called the mutual inductance and is defined as,

$$M_{i,k} = \frac{\mu_k}{4\pi} \oint_L \frac{dL_i dL_k}{r_{i,k}} \tag{8}$$

where $r_{i,k}$ is the separation distance between differential length elements dL_i and dL_k. The discretization of Eq. (7) leads to a set of simultaneous algebraic linear equations that can be solved to compute the distribution of current density in the coil and in the Pt-sample, if the external voltage is known. For the Pt-specimen $V = 0$, but for the coil $V \neq 0$ and furthermore it is difficult to measure due to the configuration and size of the coil. Additionally, as seen in Fig. 2, the Pt-specimen is asymmetrically placed along the z-direction between turns 1 and 2 of the coil, causing $V_1 \neq V_2$.

To solve this electromagnetic field and inverse heat conduction problem, for the combined heat flux extracted from the sample surface, the first step involved guessing V_1 and V_2 values, computing the current density distribution according to Eq. (7), and then evaluating the resulting RMS current from Eq. (6). If the absolute value of the difference between the calculated RMS current, I_c, and the measured one, I_m, was smaller than 1 A, the electromagnetic problem was solved. If not, the procedure was repeated. Once the electromagnetic problem converged, the source term was evaluated from Eq. (2) to start the solution of the heat transfer problem defined by Eq. (1). The solution began by guessing a combined heat transfer coefficient, h_c, to compute the temperature T_c for comparison against the measured temperature, T_m, and if the absolute difference was smaller than 1 °C, a converged h_c was obtained. Since the electrical conductivity of the Pt is a function of T, as seen in Table 1, the electromagnetic field problem was solved once again to verify that $|I_c - I_m| < 1$ A. If this criterion was met the required solution for the whole problem was reached, if not the entire solution procedure was repeated until both electromagnetic and temperature fields converged. This procedure was carried out at each temperature step along the heating and cooling trajectories indicated in Section 2.1. The set of simultaneous algebraic equations appearing in Eq. (7) was solved with the aid of LU decomposition, the magnitude of the total current in Eq. (6) was calculated by integrating the terms on the right hand side using the trapezoidal rule and Eq. (1) was solved using the finite control volume method. Further details of the solution of the equations are reported elsewhere [62].

2.4. Reference measurements

Calculating the heat transfer from the active surface of the Pt-specimen requires a good knowledge of the material properties in the test-assembly and of the boundary conditions at the other surfaces. To verify how close this requirement was met, tests were first run with a dry system, i.e., a system that excluded air-mists or

Please cite this article in press as: C.A. Hernández-Bocanegra et al., Measurement of heat flux in dense air-mist cooling: Part I – A novel steady-state technique, Exp. Therm. Fluid Sci. (2012), http://dx.doi.org/10.1016/j.expthermflusci.2012.06.015

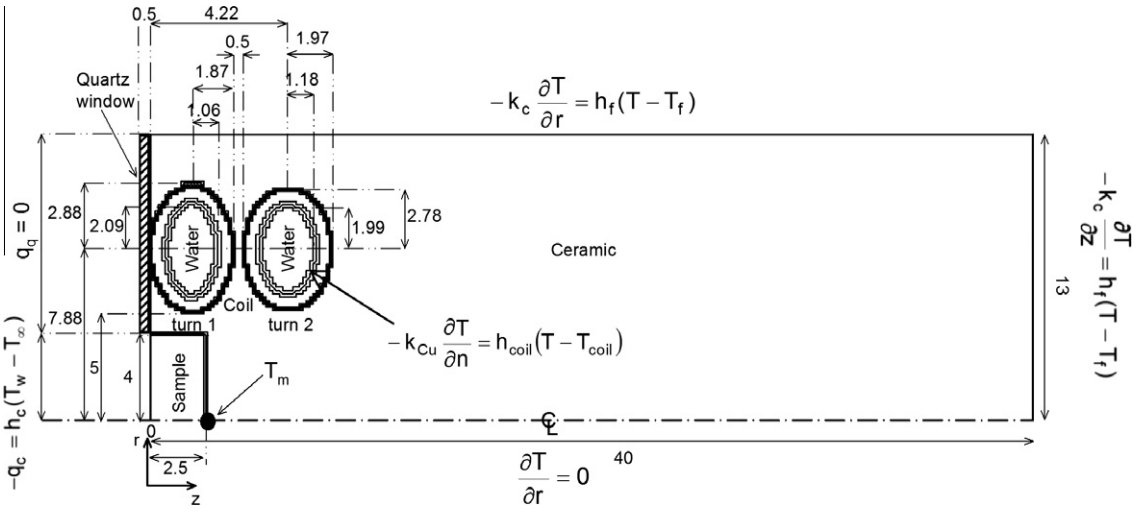

Fig. 2. Schematic of the computational domain and boundary conditions; the dimensions are given in mm.

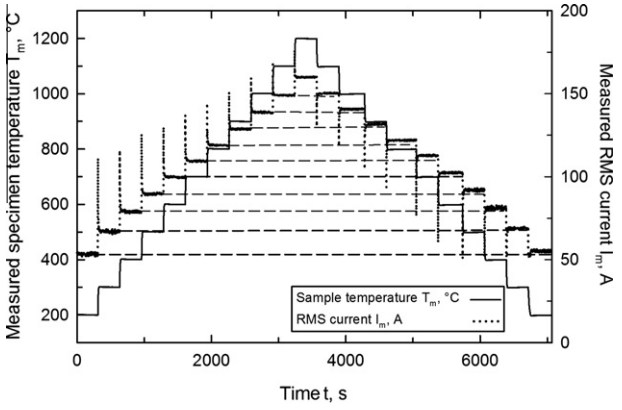

Fig. 3. Sample temperatures and RMS currents measured during a dry experiment.

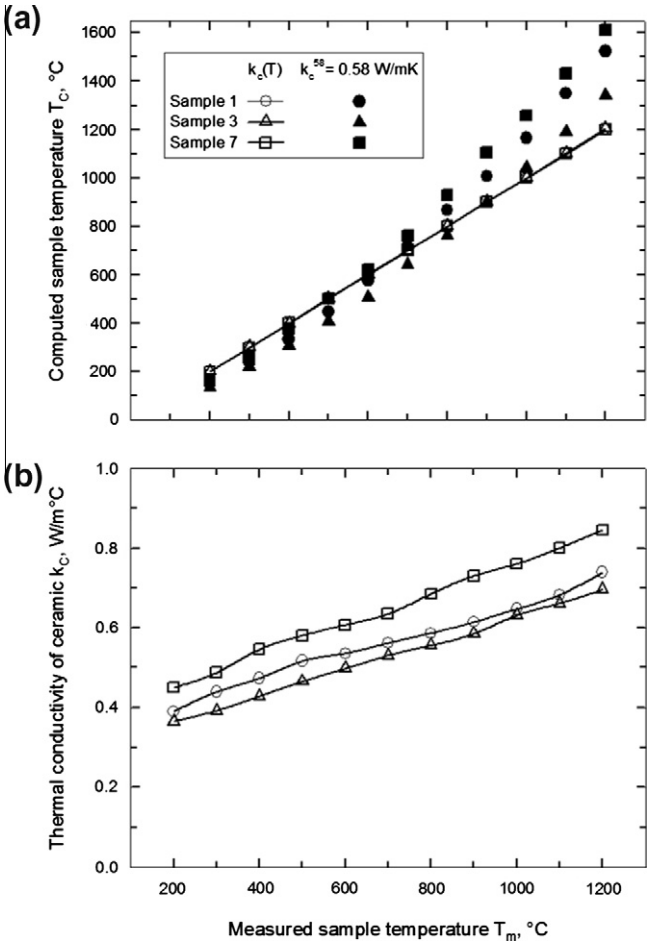

Fig. 4. (a) Comparison between measured and computed sample temperatures using both the constant and the fitted $k_c(T)$ conductivity values and (b) fitted ceramic conductivity values, for dry tests with three different probes.

water-sprays so that $q = 0$ in Eq. (3). The dry tests were run like the wet experiments by controlling the induction heating to keep the sample temperature, T_m, constant, while monitoring the heat losses. In the dry tests, the set-point in the controller was raised from 200 °C to 1200 °C and back to 200 °C, in steps of 100 °C each lasting ~300 s. Fig. 3 shows the T_m and I_m data collected. Soon after each change in set-point, the RMS current in the coil is seen to shoot to a maximum or minimum, depending on the trajectory, and then quickly approaches a nearly steady value, which persists with small fluctuations. Meanwhile, the sample temperature rapidly raises or lowers to the set-point value and stays very stable. As expected, after complete equilibration of the test-assembly, the currents I_m required to achieve a given thermal state, were approximately the same for the upward and downward trajectories, as indicated by the horizontal dashed lines. Step durations smaller than 180 s led to large differences in the I_m currents associated with a given temperature in the upward and downward branches, while time spans larger than 300 s made no difference. Thus, transient effects were important for step times smaller than 180 s but not for steps longer than 300 s. To calculate the source term in Eq. (1), the current density distribution needed for the computational procedure described in Section 2.3, was found by averaging I_m over the last 60 s of each step.

Using the properties in Table 1, the results of the calculations for these dry tests showed that the thermal energy balance closed to better than 0.01%. However, the calculated sample temperatures, T_c, departed from the measured values by as much as 400 °C as seen in Fig. 4a for T_m = 1200 °C, for the example of Sample 7. Although several parameters (e.g., ε_{Pt}, k_{Cu}, k_{Pt}, k_c, h_f, h_{coil}) could be responsible for this discrepancy, the most probable was the conductivity of the ceramic k_c, for which a single value was available

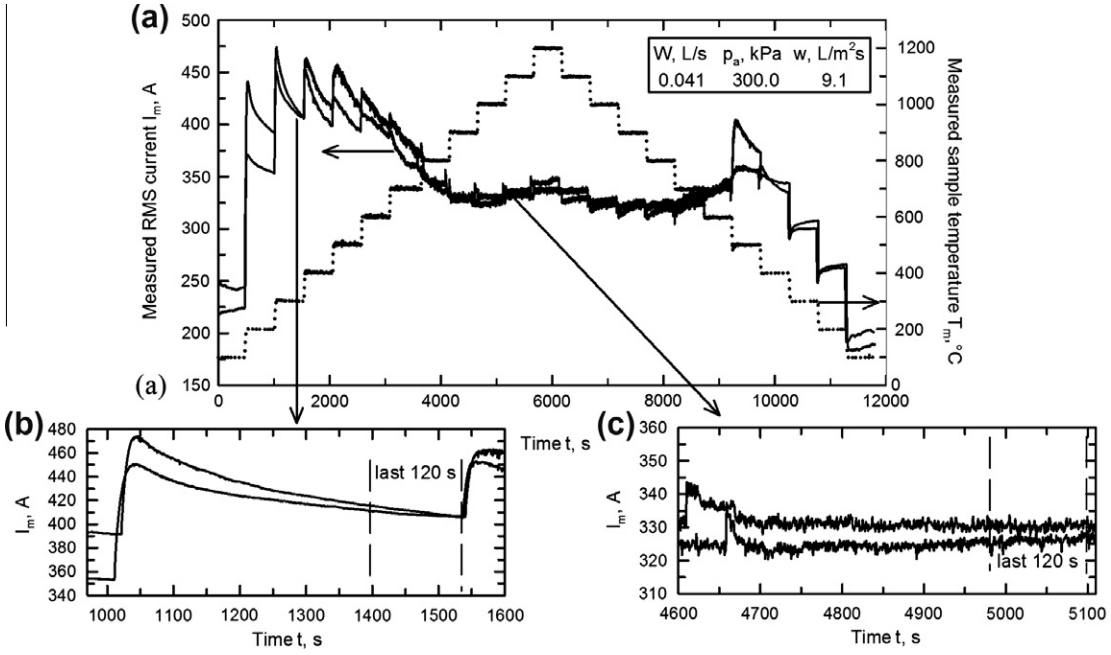

Fig. 5. Sample temperatures and RMS currents measured during wet experiments.

[58] as seen in Table 1. It is well known that the thermal conductivity of SiO_2-based materials depends on both temperature and porosity of the ceramic body. Therefore, the heat conduction model was run to find the variation of k_c as a function of temperature that satisfied simultaneously the conservation of energy and the measured sample temperatures, for each of the probes. Typical comparisons between measured and computed temperatures are plotted in Fig. 4a for three different assemblies for which the corresponding fitted ceramic conductivities as a function of T were used in estimating T_c. The empty symbols show that excellent agreement was achieved. The $k_c(T)$ values are displayed in Fig. 4b to show the typical range of variability in k_c for different ceramic bodies; it is seen also that the conductivity provided by the supplier [58] fell within the range of the estimated values.

The variation in $k_c(T)$ among the different test-assemblies suggests differences in the degree of porosity of the cast ceramic monoliths and shows the importance of characterizing each one of them, in order to maximize accuracy and to improve reproducibility in the heat fluxes measured under identical spray cooling conditions. In addition, to assess the influence of the electromagnetic field on the measured sample temperature, solitary thermocouples wires were subjected to electromagnetic fields of similar strength to those used in the dry experiments, i.e., of equal I_m current. Just a slight heating was noticed. This heating could affect the sample measurement during the transition between set-points but not after steady-state is established. Under steady conditions, the thermocouple and the Pt-sample should be in thermal equilibrium.

2.5. Data reduction and experimental uncertainty in heat flux determination

The heat flux associated with boiling convection from the surface of the Pt-specimen, $-q$, was computed according to the procedure described in Section 2.3, based on the temperature of the sample and the RMS current flowing through the coil, once steady-state had been reached. Fig. 5a shows typical recorded signals for T_m and $|I_m|$ for a spray cooling experiment involving a water flow rate of 0.041 L/s and an air inlet pressure of 300 k Pa. In this test, the sample was aligned with the nozzle axis and the water impact density was 9.1 L/m^2 s. This figure compares measurements of two replicate experiments involving different specimen assemblies and it is clear that the sample temperature was made to vary in stepwise fashion like in the dry experiments. From the comparison of these and other I_m traces covering the range of conditions studied, the measurements were found to exhibit good reproducibility, with variations generally within ±4% of the average. This suggests that the variations observed between different experimental runs must be associated with discrepancies in the water and air flow rates, as well as in the positioning of the probe relative to the nozzle axis. The temperature was held for ~480 s, at each step, to stabilize the current for a given temperature set-point. Therefore, the RMS coil current used to estimate the boiling heat flux, according to the procedure described in Section 2.3, corresponded to the average value of the signals recorded in the last 120 s, as shown in Fig. 5b and c.

From Sections 2.3 and 2.4, once the boundary conditions and the thermophysical properties have been properly assessed, the estimated boiling heat flux, $-q$, depends on the evaluation of the source term Q_v, given by Eq. (2), and on the measured sample temperature, T_m. Therefore, the uncertainty in $-q$ is due to factors affecting the electromagnetic induction in the sample (e.g. measured coil RMS current, coil radius, sample radius and sample thickness), the thermocouple error and the uncertainty in the thermocouple position. Using the electromagnetic and heat conduction model and following the method proposed by Kline and McClintock [63], Table 2 shows the expected contributions that typical variations of the different independent variables would have on the uncertainty in $-q$. This table shows that the largest contributors to the uncertainty in the heat flux are the coil radius and the sample radius. Therefore accurate measurement of these two variables is essential, but without overlooking control of the other variables. As seen in the table, the overall uncertainty is estimated to be around 9%. This result agrees well with the majority of experimental errors obtained among repetitions of experiments carried out under the same conditions (i.e., same nozzle, W, p_a and nozzle position) as shown in Fig. 6. In this figure the experimental uncertainty among repetitions (defined as the ratio between the maximum difference among measurements over their average value)

Please cite this article in press as: C.A. Hernández-Bocanegra et al., Measurement of heat flux in dense air-mist cooling: Part I – A novel steady-state technique, Exp. Therm. Fluid Sci. (2012), http://dx.doi.org/10.1016/j.expthermflusci.2012.06.015

Table 2
Uncertainty analysis for boiling heat flux.

Independent variable		$\left\|\frac{\delta x_i}{q}\frac{\partial q}{\partial x_i}\right\| \times 100\,(\%)$
x_i	Error (δx_i)	
RMS current I_m (A)	3	2
Coil radius (mm)	0.2	6.4
Sample radius (mm)	0.05	5
Sample thickness (mm)	0.05	1.2
Sample temperature T_m (°C)	2.0	0.05
Off-center thermocouple position (mm)	1	0.1
Total uncertainty	$(\delta q/q) \times 100 = 9.4\%$	

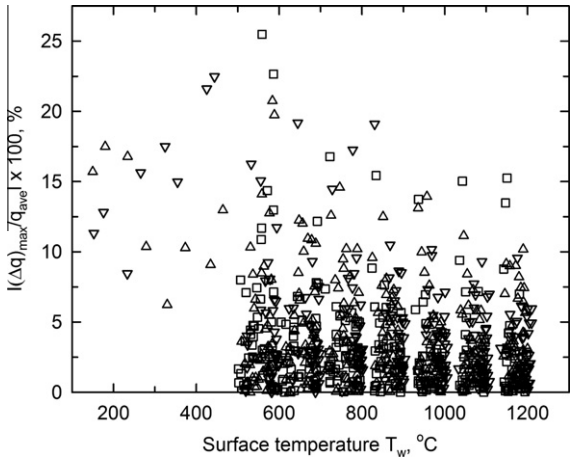

Fig. 6. Experimental uncertainty of the measured heat flux at different surface temperatures and for the different nozzle conditions studied.

is plotted for the different estimated surface temperatures; each dot in the plot corresponds to a single set of conditions which are defined and further evaluated in Part II of the article [1]. The repetitions were consecutive and non-consecutive using the same or different test-assemblies. When a probe was changed, a previously investigated condition was selected randomly to verify repeatability of the measurements.

3. Evaluation of measuring system

To assess the heat flux measuring system, a 90° fan-discharge W19822 air-mist nozzle was studied, according to the arrangement shown in Fig. 1. As seen in this figure, the measuring sample was much smaller than the cross section of the mist jet, so the heat flux measurements varied with spatial position within the jet, according to the local water impact density, w, the local volume mean diameter, d_{30}, and the local normal volume weighted mean velocity, $u_{z,v}$. By measuring average heat flux over the sample surface area, this system can provide a spatial resolution of ~8 mm, which is sufficient to resolve the large-scale spatial variations of heat flux with commercial nozzles, whilst avoiding the small-scale variations caused by individual droplets [3,32]. The w was determined with a patternator and d_{30} and $u_{z,v}$ using a particle/droplet image analyzer [1]. For the case reported in Figs. 7–10 and 12, the mist parameters were: $w = 9.1$ L/m^2 s, $d_{30} = 30.91$ μm and $u_{z,v} = 28.7$ m/s. Appendix A presents the size and velocity distributions of the drops passing through the sampling volume located around the position at which $-q$ was determined, and gives the definitions of the average mist parameters used. The size and velocity distributions were measured in free non-impinging air-mist jets, which are described in further detail with other results in Part II of this work [1].

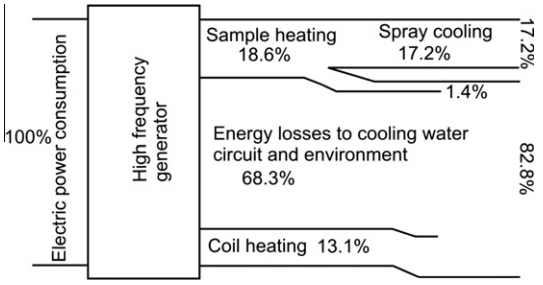

Fig. 7. Sankey diagram of the power distribution for the system generator – test-assembly, with $-q = 9.2$ MW/m^2 for conditions: $W = 0.076$ L/s, $p_a = 412$ k Pa, $T_w = 519.6$ °C, $T_m = 600$ °C and $w = 22$ L/m^2 s.

Fig. 8. Computed thermogram in the probe for $W = 0.041$ L/s, $p_a = 300$ k Pa and $T_m = 1200$ °C.

3.1. Heat balance and thermal state of the test-specimen assembly

Adequate performance of the probe developed here to measure the spray heat flux relied on maintaining steady-state thermal conditions despite the intense cooling. This rested on selecting an appropriate metal for the sample, adequate size and geometry for the metal specimen and coil, and on providing good insulation of the inactive surfaces. The Sankey diagram displayed in Fig. 7 shows an example of how the total power applied by the generator (2756 W) was distributed in the system for a case where the heat extracted by the spray was 9.2 MW/m^2. Even for the high power demanded for this case, only 55.1% of the capacity of the generator was required. Hence, for the probe design in Fig. 2, the induction system had enough capacity to investigate a wide range of spray cooling conditions, as seen in Part II of the article where heat fluxes as large as ~12 MW/m^2 were estimated for certain spraying conditions [1]. From the mutual inductance method, described in Section 2.3, it was calculated that 31.7% of the power demanded was used to supply heat to the Pt-disk and the two-turns of the coil, as also can be seen in Fig. 7. The rest of the power was dissipated into the electric and electronic components of the generator and ultimately into the water of the cooling circuit or directly to the environment. Additionally, it should be mentioned that of the total Joule power generated in the specimen and in the coil, 54.2% was removed by boiling convection and radiation from the active surface of the Pt-sample, 45.7% by convection to the coil cooling water and 0.1% by natural convection from the inactive surfaces. The proximity of the coil turns to the specimen caused some of the heat generated in the specimen to be lost to the water circulating in the coil, as seen in Fig. 7.

Fig. 8 shows the typical computed temperature distribution throughout the probe, for a case where the Pt-specimen was spray

Please cite this article in press as: C.A. Hernández-Bocanegra et al., Measurement of heat flux in dense air-mist cooling: Part I – A novel steady-state technique, Exp. Therm. Fluid Sci. (2012), http://dx.doi.org/10.1016/j.expthermflusci.2012.06.015

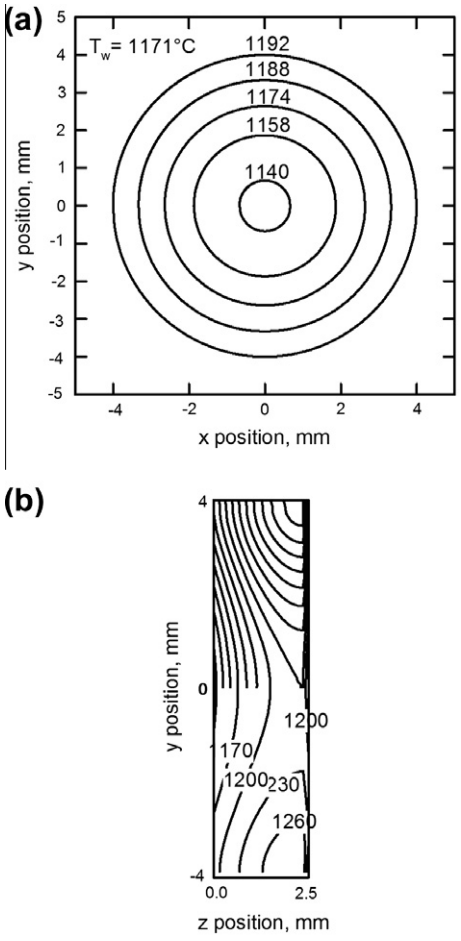

Fig. 9. Temperature contours in (a) surface and (b) symmetry plane of the Pt-sample, for W = 0.041 L/s, p_a = 300 k Pa and T_m = 1200 °C.

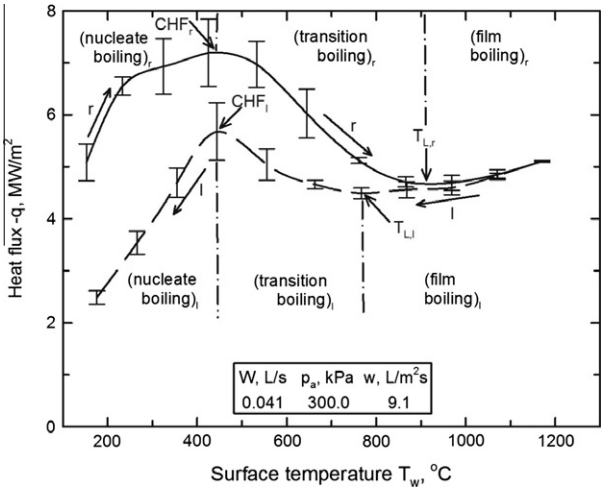

Fig. 10. Boiling curves for a thermal loop with T_m between 200 °C and 1200 °C.

cooled while its control temperature T_m was maintained at 1200 °C, for W = 0.041 L/s and p_a = 300 k Pa. This figure depicts the large temperature gradient in the thinnest ceramic region between the Pt-disk and coil that leads to the transfer of heat from the sample to the coil cooling water. Everywhere else, the ceramic insulated the specimen adequately. The calculated temperature field inside the Pt-specimen can be better appreciated from Fig. 9a and b, which shows temperature contours for the front face and symmetry plane of the disk, respectively. As Fig. 9a indicates, according to the electromagnetic and heat conduction model, the active surface of the sample exhibits significant temperature variations, so the following sections use the area-averaged surface temperature to relate with the spray heat flux extracted from the surface.

3.2. Boiling curves

The I_m traces plotted in Fig. 5a, for a typical spray cooling experiment, reveal that in the range from 200 °C to 800 °C, the currents needed to maintain a given sample temperature are significantly different for the temperature raising and temperature lowering paths of the loop cycle; the difference is particularly evident at lower temperatures. From the figure, it is observed that the RMS current needed to maintain a given sample temperature was larger during the stepwise ascent than it was in the descent path. These results suggest higher boiling heat fluxes during the raising path, which required the generator to supply a larger current to maintain a given surface temperature. These history-dependent differences in heat transfer are known as boiling hysteresis [43,44,53] as indicated in Section 1. An additional feature that can be observed on Fig. 5a is that above 900 °C, the coil currents were very similar along both trajectories. This behavior hints that the same boiling phenomena prevail along both paths, and hence hysteresis was negligible above this temperature.

Fig. 10 shows the boiling curves calculated from the I_m measurements presented in Fig. 5a. The boiling heat flux values plotted in this figure correspond only to the boiling convection component $-q$, since the radiation part of Eq. (3) was subtracted. From Fig. 10, it is seen that in the nucleate and transition boiling regimes, the heat flux during the temperature raising path, r, is considerably higher than for the lowering path, l; but both curves are close in the stable film boiling regime. It is noticed from the figure that the uncertainty bars for the r and l curves do not overlap along the nucleate and transition regimes, which implies that the differences between the two curves are real, due to hysteresis phenomena. The high boiling curve for the temperature raising path suggests that in the nucleate boiling regime when the Pt surface starts at ~200 °C (i.e. at the lower surface superheat used) the impingement of fine high-velocity droplets should flood the surface with a thin layer of water. This water film must interact intensively with the surface, promoting the quick formation of vapor bubbles on certain surface sites, causing high heat extraction. It could be conjectured that the frequent impingement of fast drops over the liquid film would promote the release of the vapor bubbles formed, the renewal of liquid in contact with the surface and the mixing of the liquid film, to explain the enhanced heat transfer. At higher temperatures, more surface sites should become active for the nucleation of vapor bubbles, leading to increased heat removal until reaching the critical heat flux CHF$_r$. Once the temperature corresponding to the CHF$_r$ is exceeded, a transition boiling regime appears with the formation of vapor patches. The patches hinder direct contact of the liquid with the surface, thereby reducing the heat flux. At the Leidenfrost temperature, $T_{L,r}$, the minimum $-q$ is reached with the formation of a stable vapor film. Further increase in the surface temperature causes a slight increase in the heat flux due to the increasing temperature gradient across the vapor film.

Fig. 10 shows that along the temperature lowering trajectory from 1200 °C to 200 °C, the l and r boiling curves matched very closely at the highest temperatures but separate at ~800 °C, with the l curve remaining below the r curve along the rest of the path. This suggests that patches of the vapor film persist to lower temperatures along the temperature decreasing path. Below the $T_{L,l}$ tem-

perature, the heat flux increases until it attains the critical value, CHF_l. This increase in heat flux may be associated to an increase in the contact area of liquid films with the surface which could promote the resumption of nucleate boiling that could become more abundant as the temperature decreases. However, apparently the direct contact of liquid with the surface is difficult and rare because the CHF_l is considerably smaller than the CHF_r. The lower magnitude of the critical heat flux for the descending path suggests, as mentioned, that patches of vapor film that form at higher temperatures are able to survive, thereby hindering liquid contact with the surface. Upon entering the nucleate boiling regime, the difference between the heating and cooling paths increases. This behavior advices a poor wetting of the surface during cooling, relative to that suggested by the high heat fluxes registered along the *r* branch.

The hysteresis phenomena found in this investigation exhibits certain resemblance with that reported by Witte and Lienhard [49] and Rajab and Winterton [52], who also found two transition boiling curves, with the temperature–rising curve located above the temperature–lowering curve, like that observed in Fig. 10. However, in addition to two transition boiling curves, the current study also reveals differences between the curves in the nucleate boiling regime. The temperature–rising nucleate boiling curve in Fig. 10 has much higher heat fluxes than the temperature–lowering curve. As mentioned in Section 1, Rajab and Winterton [52] measured the liquid contact in their pool boiling system that operated up to $T_w \approx 320$ °C. They suggested that heating transition is a boiling regime with unstable vapor patches and that cooling transition boiling is a regime with bigger patches that depress the boiling heat flux, and that this phenomenon persists until the CHF is reached, after which normal nucleate boiling is reestablished. However, for the conditions studied here, the results hint that also in the nucleate boiling regime with temperature lowering, the nucleation and growth of bubbles takes place over a reduced liquid–surface contact area, so large vapor patches are preserved from higher temperatures. The phenomena that are conjectured to occur along the regimes of the *r* and *l* boiling curves are schematically illustrated in Fig. 11. The irregular liquid layer impinged by drops shows vapor bubbles and vapor patches which are less and more numerous, respectively, in the *l* than in *r* path, for the

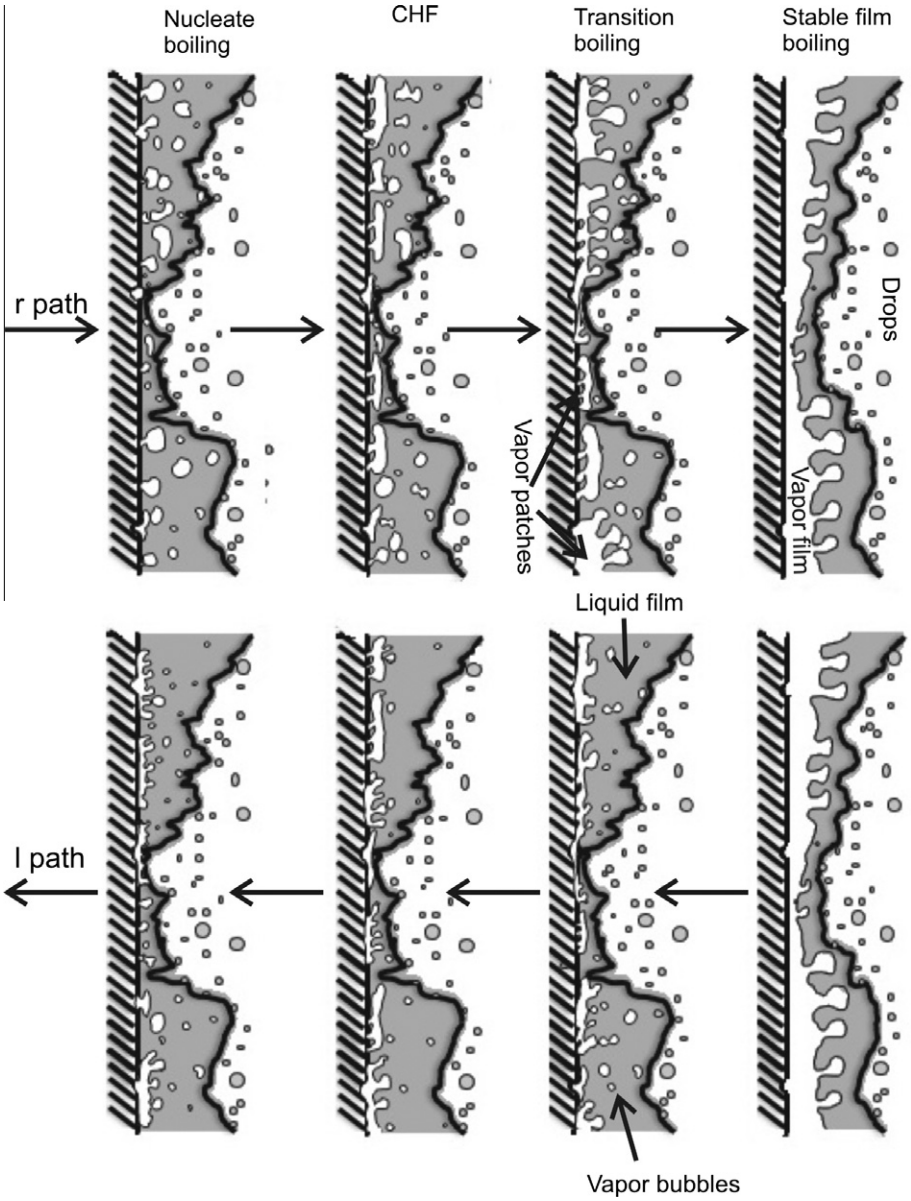

Fig. 11. Schematic representation of various boiling regimes along the temperature rising, *r*, and lowering, *l*, paths of Fig. 10.

Please cite this article in press as: C.A. Hernández-Bocanegra et al., Measurement of heat flux in dense air-mist cooling: Part I – A novel steady-state technique, Exp. Therm. Fluid Sci. (2012), http://dx.doi.org/10.1016/j.expthermflusci.2012.06.015

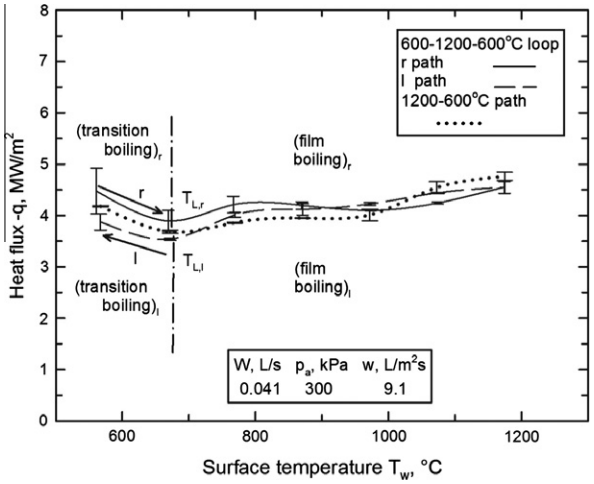

Fig. 12. Boiling curves for thermal loops with T_m 600–1200–600 °C and for thermal paths 1200–600 °C.

nucleate regime, the CHF point and the transition regime; the schematics, shown in the figure, for the film boiling regime are alike along both paths.

The Pt samples used in this work had an initially even and clean surface that got rough and slightly coated by salts as the experiments proceeded, additionally a Pt surface is hydrophilic [64] like many oxidized surfaces of other metals are (e.g. Fe) [65]. These surface characteristics – roughness, hydrophilic nature and contamination – have been reported to favor hysteresis [47,48,52,53]. Thus, it is possible that the hysteresis behavior was not reported in the steady-state spray cooling investigations cited in Section 1 simply because the techniques were unable to follow temperature increase and temperature decrease paths or because they included only a narrow temperature range. Also, the unsteady-state techniques under free cooling conditions, that have been employed, are inherently unable to reveal the boiling hysteresis phenomenon. The existence of hysteresis points out the difficulties that may be found in simulating actual cooling processes in the laboratory, since the thermal response of the system, in the nucleate and transition boiling regimes, depends on the initial thermal state of the surface and on its history. Fortunately, hysteresis was absent at the highest temperatures.

Since the main interest behind this work is the spray cooling of highly superheat surfaces with T_w between 700 °C and 1200 °C, boiling curves in this temperature range were investigated further. The solid and dashed lines in Fig. 12 show boiling curves for the thermal loop 600–1200–600 °C corresponding to the same spraying conditions as those used in Fig. 10. From the solid and dashed lines in Fig. 12, it is seen that for T_w ranging between 550 and 1200 °C the hysteresis phenomenon was essentially absent, as indicated by the negligible separation between the raising and lowering curves of the loop. It is appreciated that these boiling curves comprised transition and stable film boiling regimes, as suggested by the different slopes of the curves over different temperature ranges. Comparing Figs. 10 and 12 over the T_w interval of 550 °C to 1200 °C reveals that the *r* and *l* boiling curves appearing in Fig. 10 exhibit significant differences in the range of 550 °C to 800 °C, which are not present in the curves plotted in Fig. 12. Additionally, the heat fluxes for the 600–1200–600 °C loop are smaller than the corresponding high-temperature heat fluxes from the 200–1200–200 °C loop. This result hints that when the thermal cycle starts at a sufficiently high temperature, e.g., 600 °C, the nucleation and growth of the vapor bubbles occurs fast, forming vapor patches that hinder the direct contact of the liquid with the solid surface. In contrast, starting the thermal cycle at low T_w, e.g., ~200 °C, apparently enables the liquid water to fully wet the surface causing a persistent liquid layer that leads to more intense heat extraction later at the higher temperatures. These results clearly show the importance of fully understanding, the thermal history in the actual processes, in order to simulate them accurately in the laboratory. The dotted line in Fig. 12 shows that the boiling curve for the thermal path 1200–600 °C, falls quite close to the loop curves. Thus, for sufficiently high temperatures the initial temperature and thermal history have negligible effect on the spray cooling of the sample. Part II of this two-part article further investigates and quantifies the effect of the spray parameters on the boiling heat extraction for high sample temperatures, T_m, between 600 and 1200 °C [1].

4. Summary and conclusions

A novel steady-state method based on induction heating has been developed for studying the heat transfer characteristics of highly superheated surfaces subjected to intense spray cooling conditions, such as those found in steel continuous casting and other processes. To our best knowledge, this is the first time that a steady-state method has been successfully applied under such demanding heat extraction conditions.

The technique measures the heat flux extracted when a local region of the spray from a water–air–mist nozzle impinges upon the active surface of a hot Pt-disk, which is encircled by an induction coil, both of which are embedded in a cast ceramic monolith that shields the other surfaces from the spray. A digital controller adjusts the output power of a high-frequency generator to balance the induction heating of the metallic sample with the heat removed by the boiling of spray droplets impinging on its active surface, in order to maintain the control temperature of the sample at the desired set-point. Measurement of the RMS current flowing through the coil to maintain the sample temperature, together with the solution of a two-dimensional axi-symmetric computational model of the electromagnetic and heat conduction equations, enabled estimation of the heat extracted locally by the spray. The present steady-state technique allows determining the boiling curve in the temperature range of 200–1200 °C under intense spraying conditions of practical interest in the cooling of surfaces with large superheat.

A rigorous experimental procedure involving stepwise heating and cooling over the 200–1200 °C temperature range enabled the complete boiling curves to be determined for both trajectories. The results reveal that boiling hysteresis occurs in the nucleation and transition boiling regimes, and that this behavior is almost absent in the stable film boiling regime. The large list of factors that may lead to boiling hysteresis clearly points to the need for understanding the phenomena involved in the extraction of heat, in order to enable laboratory simulation of the cooling conditions that take place in industrial processes. The characteristics of the present technique, which enables maintaining a metallic sample at a chosen temperature for prolonged periods of time while being subjected to intense heat extraction, opens the possibility for careful examination of the phenomena occurring during spray cooling by dense sprays. In the interval involving temperatures only between 600 and 1200 °C hysteresis is absent and for this range the influence of spray parameters on heat transfer is examined in Part II of this article [1].

Acknowledgements

We are grateful to the National Council of Science and Technology of Mexico (CONACYT) and the National Science Foundation (US) for financial support through Grants Nos. 57836 and

CMMI-0900138, respectively, and also to the Continuous Casting Consortium at the University of Illinois. CAH and XZ wish to thank CONACYT and the CCC, respectively, for their scholarship grants. We want to recognize the valuable contributions of Mr. Sami Vapalahti in the initial stages of the project. The excellent technical support of Mr. Jorge Ramos of ASEPSA S.A. de C.V. is greatly appreciated.

Appendix A

Fig. A.1a and b shows distributions of the size and velocity of drops in samples of at least 6000 drops passing through a sampling volume centered around $x = 0$ m at $y = 0$ m and $z = 0.19$ m, for the indicated nozzle operating conditions. As is typical of all the nozzle types and operating conditions used in this work, Fig. A.1a shows that the number frequency distribution of droplet diameter is strongly skewed to the right, indicating that small-size droplets are very numerous and that the large ones ($d_d \geqslant 62.5$ μm for the case illustrated) are very scarce. Nonetheless, the volume frequency distribution indicates that these larger size droplets contribute very importantly to the volume of water passing through the sampling volume. On the other hand, the droplet velocity tends to be normally distributed as indicated in Fig. A.1b. Since, it is generally agreed that the volume of water arriving to the hot surface plays a very important influence on heat transfer the diameter and velocity of the droplets were characterized by the droplet volume mean diameter,

$$d_{3,0} = \left(\sum_{i=1}^{N} d_{d,i}^3 / N \right)^{1/3} \tag{A.1}$$

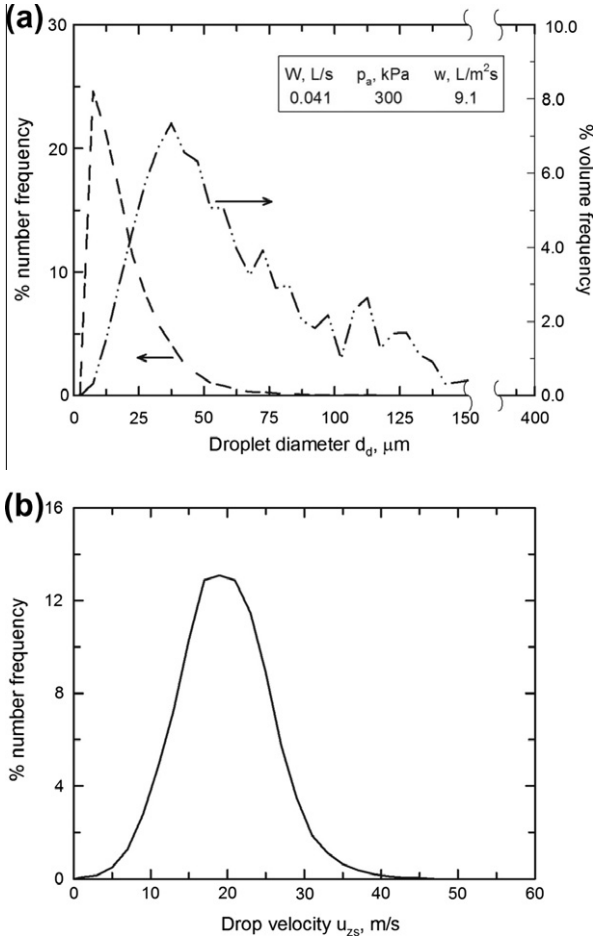

Fig. A.1. Measured: (a) drop size number and volume frequency distributions and (b) drop velocity number frequency distribution.

and the normal volume weighted mean velocity,

$$u_{z,v} = \sum_{i=1}^{N} u_{z,i} d_{d,i}^3 \Big/ \sum_{i=1}^{N} d_{d,i}^3 \tag{A.2}$$

where $d_{d,i}$ and $u_{z,i}$ are the diameter and normal velocity to the surface of drop i in a sample of N droplets.

The water impact density distribution was measured by local sampling of the flux of spray impinging upon a surface with an array of collection tubes with small openings. Details of the measuring techniques are given elsewhere [1].

References

[1] C.A. Hernández B., A.H. Castillejos E., F.A. Acosta G., X. Zhou, B.G. Thomas, Measurement of heat flux in dense air-mist cooling: Part II. The influence of mist characteristics on steady-state heat transfer, Experimental Thermal and Fluid Science (2012), http://dx.doi.org/10.1016/j.expthermflusci.2012.06.007.
[2] S. Deb, S-C. Yao, Analysis on film boiling heat transfer of impacting sprays, International Journal of Heat Mass Transfer 32 (11) (1989) 2099–2112.
[3] B. Abbasi, J. Kim, A. Marshall, Dynamic pressure based prediction of spray cooling heat transfer coefficients, International Journal of Multiphase Flow 36 (8) (2010) 491–502.
[4] W.M. Rohsenow, H. Choi, Heat, Mass and Momentum Transfer, thirteenth printing., Prentice-Hall, NJ, 1961. pp. 211–236.
[5] J.E. Camporredondo S, A.H. Castillejos E, F.A. Acosta G, E.P. Gutiérrez M, M.A. Herrera G, Analysis of thin slab casting by the compact-strip process: Part I. Heat transfer and solidification, Metallurgical and Materials Transactions B 35 (3) (2004) 541–559.
[6] J. Sengupta, B.G. Thomas, M.A. Wells, The use of water cooling during continuous casting of steel and aluminum alloys, Metallurgical and Materials Transactions B 36 (1) (2005) 187–204.
[7] D. Hall, I. Mudawar, R.E. Morgan, S.L. Ehlers, Validation of a systematical approach to modeling spray quenching of aluminum alloys extrusions, composites and continuous castings, in: Proceedings of the Second International Conference on Quenching and the Control of Distortion, Cleveland, Ohio, 1996, pp. 473–487.
[8] G.E. Totten, C.E. Bates, Handbook of Quenchants and Quenching Technology, first printing., ASM Int., Ohio, 1993. pp. 238–287.
[9] M. Tanaka, Heat transfer of a spray droplet in a nuclear reactor containment, Nuclear Technology 47 (2) (1980) 268–281.
[10] H. Anglart, F. Alavyoon, R. Novarini, Study of spray cooling of a pressure vessel head of a boiling water reactor, Nuclear Engineering and Design 240 (2) (2010) 252–257.
[11] G.P. Celata, M. Cumo, A. Mariani, L. Saraceno, A comparison between spray cooling and film flow cooling during the rewetting of a hot surface, Heat Mass Transfer 45 (7) (2009) 1029–1035.
[12] S. Martorano, Spray nozzles selections for water spray systems: Options and applications explained, International Fire Protection 41 (2010) 30–33.
[13] G.P. Celata, M. Cumo, C. Lombardo, A. Mariani, L. Saraceno, Experimental result on rewetting of hot surfaces by droplet impingement, Experimental Thermal and Fluid Science 29 (3) (2005) 275–285.
[14] T. Cader, L.J. Westra, R.C. Eden, Spray cooling thermal management for increased device reliability, IEEE Transactions on Device and Materials Reliability 4 (4) (2004) 605–613.
[15] M. Fabbri, S. Jiang, V.K. Dhir, A comparative study of cooling of high power density electronics using spray and microjets, Transactions of the ASME 127 (1) (2005) 38–48.
[16] B.M. Pikkula, J.H. Torres, J.W. Tunnell, B. Anvari, Cryogen spray cooling: effects of droplet size and spray density on heat removal, Lasers in Surgery and Medicine 28 (2) (2001) 103–112.
[17] E. Karapetian, G. Aguilar, S. Kimel, E.J. Lavernia, J.S. Nelson, Effects of mass flow rate and droplet velocity on surface heat flux during cryogen spray cooling, Physics in Medicine and Biology 48 (1) (2003) N1–N6.
[18] K.M. Graham, S. Ramadhyani, Experimental and theoretical studies of mist jet impingement cooling, Journal of Heat Transfer 118 (2) (1996) 343–349.
[19] F.K. McGinnis, J.P. Holman, Individual droplet heat transfer rates for splattering on hot surfaces, International Journal of Heat and Mass Transfer 12 (1) (1969) 95–108.
[20] K. Araki, S. Yoshinobu, Y. Nakatani, A. Moriyama, Stationary measurement for heat transfer coefficient in droplet-cooling of hot metal, Transactions ISIJ 22 (12) (1982) 952–958.
[21] J.D. Bernardin, I. Mudawar, Film boiling heat transfer of droplet streams and sprays, International Journal of Heat and Mass Transfer 40 (11) (1997) 2579–2593.
[22] S. Toda, A study of mist cooling (1st Report: Investigation of mist cooling), Heat Transfer: Japanese Research 1 (3) (1972) 39–50.
[23] S. Ishigai, S. Nakanishi, T. Ochi, Boiling heat transfer for a plane water jet impinging on a hot surface, in: Proceedings of the Sixth International Heat Transfer Conf., Hemisphere Pub. Corp., Toronto, Canada, 1978, pp. 445–450.
[24] W.M. Grissom, F.A. Wierum, Liquid spray cooling of a heated surface, International Journal of Heat and Mass Transfer 24 (2) (1981) 261–271.

[25] R. Jeschar, U. Reiners, R. Scholz, Heat transfer during water and water–air spray cooling in the secondary cooling zone of continuous casting plants, in: R.W. Stovall (Ed.), Proceedings of the Fifth International Iron and Steel Congress, Iron and Steel Society, Washington DC, 1986, pp. 511–521.
[26] I. Mudawar, W.S. Valentine, Determination of the local quench curve for spray-cooled metallic surfaces, Journal of Heat Treating 7 (2) (1989) 107–121.
[27] V. Heidt, R. Jeschar, Influence of running water on the heat transfer in continuous casting, Steel Research 64 (3) (1993) 157–164.
[28] I. Stewart, J.D. Massingham, J.J. Hagers, Heat transfer coefficient effects on spray cooling, Iron and Steel Engineer 73 (7) (1996) 17–23.
[29] J.C. Fry, H.D. Morgan, W.D. Morris, J.O. Medwell, Design of steady state test apparatus to evaluate heat transfer coefficient of spray, Ironmaking and Steelmaking 24 (1) (1997) 47–52.
[30] J. Schmidt, H. Boye, Influence of velocity and size of the droplets on the heat transfer in spray cooling, Chemical Engineering Technology 24 (3) (2001) 255–260.
[31] W. Jia, H.-H. Qiu, Experimental investigation of droplet dynamics and heat transfer in spray cooling, Experimental Thermal and Fluid Science 27 (7) (2003) 829–838.
[32] B. Horacek, K.T. Kiger, J. Kim, Single nozzle spray cooling heat transfer mechanisms, International Journal of Heat and Mass Transfer 48 (8) (2005) 1425–1438.
[33] M.S. Jenkins, S.R. Story, R.H. David, Defining air-mist nozzle operating conditions for optimum spray cooling performance, in: Editor name (Ed.), Proceedings of the Nineteenth Australasian Chemical Engineering Conference, Institute of Engineers, Newcastle, New South Wales, Australia, September 12–20, 1991, pp. 161–169.
[34] V. Olden, M. Raudensky, K. Onsrud, W. Hummel, Water spray cooling of stainless and C–Mn steel, Steel Research 69 (6) (1998) 240–246.
[35] B. Patrick, B. Barber, Caster operation, design and maintenance to ensure high product quality, in: Proceedings of the ISSTech Conference, Iron and Steel Society, Indianapolis, IN, 2003, pp. 975–985.
[36] E.A. Mizikar, Spray cooling investigation for continuous casting of billets and blooms, Iron and Steel Engineer 47 (6) (1970) 53–60.
[37] M. Ciofalo, I. Di Piazza, V. Brucato, Investigation of the cooling of hot walls by liquid water sprays, International Journal of Heat and Mass Transfer 42 (7) (1999) 1157–1175.
[38] M. Ciofalo, A. Caronia, M. Di Liberto, S. Puleo, The Nukiyama curve in water spray cooling: its derivation from temperature-time histories and its dependence on the quantities that characterize drop impact, International Journal of Heat and Mass Transfer 50 (25–26) (2007) 4948–4966.
[39] H.M. Al-Ahmadi, S.C. Yao, Spray cooling of high temperature metals using high mass flux industrial nozzles, Experimental Heat Transfer 21 (1) (2008) 38–54.
[40] W.J.J. Vorster, S.A. Schwindt, J. Schupp, A.M. Korsunsky, Analysis of the spray field development on a vertical surface during water spray-quenching using a flat spray nozzle, Applied Thermal Engineering 29 (7) (2009) 1406–1416.
[41] A.H. Castillejos E., F.A. Acosta G., M.A. Herrera, I. Hernández C., E.P. Gutiérrez M, Practical productivity gains – Towards a better understanding of air-mist cooling in thin slab continuous casting, in: R.I.L. Guthrie, (Ed.), Proceeding of the Third International Congress of Steelmaking, Association of Iron and Steel Technology, Charlotte, NC, 2005, pp. 881–890.
[42] S. Nukiyama, Translation – the maximum and minimum values of heat Q transmitted fron metal to boiling water under atmosphere pressure, International Journal of Heat and Mass Transfer 9 (12) (1966) 1419–1433.
[43] F.P. Incropera, D.P. De Witt, T.L. Bergman, A.S. Lavine, Fundamentals of Heat and Mass Transfer, sixth ed., John Wiley & Sons, Hoboken, NJ, 2007. pp. 622–627.
[44] J.G. Collier, J.R. Thome, Convective Boiling and Condensation, third ed., Oxford University Press, NY, 1994. pp. 148–150, 163.
[45] T.B. Drew, C. Mueller, Boiling, Transactions of the American Institute of Chemical Engineers 33 (1937) 449–473.
[46] R. Hohl, H. Auracher, J. Blum, W. Marquardt, Pool boiling heat transfer experiments with controlled wall temperature transients, in: Proceedings 2nd European Thermal Science and 14th UIT Nat. Heat Transfer Conference, Edizioni ETS, Rome, 1996, pp. 1647–1652.
[47] D.W. Zhou, C.F. Ma, J. Yu, Boiling hysteresis in impinging circular submerged jets with highly wetting liquids, International Journal of Heat and Fluid Flow 25 (1) (2004) 81–90.
[48] T.M. Wojcik, Experimental investigations of boiling heat transfer hysteresis on sintered, metal – fibrous, porous structures, Experimental Thermal and Fluid Science 33 (3) (2009) 397–404.
[49] L.C. Witte, J.H. Lienhard, On the existence of two 'transition' boiling curves, International Journal of Heat and Mass Transfer 25 (6) (1982) 771–778.
[50] P.J. Berenson, Transition boiling heat transfer from a horizontal surface, MIT Heat Transfer Lab. Tech. Report no. 17, 1960.
[51] A. Sakurai, M. Shiotsu, Temperature-controlled pool-boiling heat transfer, in: Proceedings Fifth International Heat Transfer Conference, 4, B3.1, Tokyo, 1974, pp. 81–85.
[52] I. Rajab, R.H.S. Winterton, The two transition boiling curves and solid-liquid contact on a horizontal surface, International Journal of Heat and Fluid Flow 11 (2) (1990) 149–153.
[53] A. Faghri, Y. Zhang, J. Howell, Advanced Heat and Mass Transfer, first ed., Global Digital Press, Columbia, MO, 2010. pp. 705–707.
[54] A.H. Castillejos E., F.A. Acosta G., R. Santos P., E.P. Gutiérrez M., R. González de la P., Studies for the improvement of the secondary cooling system of CSP thin slab casters, in: G.A. Irons (Ed.), Proceedings of the McMaster Iron and Steelmaking Symposium, Thinner Slab Casting, McMaster University, Hamilton, Ontario, 2005, pp. 47–58.
[55] J.J. Montes R, A.H. Castillejos E, F.A. Acosta G, E.P. Gutiérrez M, M.A. Herrera G, Effect of the operating conditions of air-mists nozzles on the thermal evolution of continuously cast thin slabs, Canadian Metallurgical Quarterly 47 (2) (2008) 187–204.
[56] http://www.platinummetalsreview.com/jmpgm.
[57] http://www.ndt-ed.org/EducationResources/CommunityCollege/Materials/Physical_Chemical/Electrical.htm.
[58] High Temperature Materials Handbook, vol. 5, Cotronics Corp., 2005, pp. 23.
[59] J. Szekely, N.J. Themelis, Rate Phenomena in Process Metallurgy, John Wiley & Sons Inc., N.Y., 1971. pp. 236–239.
[60] E.J. Davies, Conduction and Induction Heating, The Institution of Engineering and Technology, London, 2007. pp. 17–18.
[61] E. Kolbe, W. Reiss, Eine Methode zur numerischen Bestimmung der Stromdichteverteilung in induktiv erwärmten Körpern unterschiedlicher geometrischer Form, Mittailung aus dem Institut für Elektrowärme 9 (3) (1963) 311–317.
[62] C.A. Hernández B., Estudio de la Extracción de Calor con Nieblas de Agua Bajo Condiciones de Estado Estacionario, Ph.D. Thesis, CINVESTAV–Unidad Saltillo, Coahuila, Mexico, August 9, 2012.
[63] S.J. Kline, F.A. McClintock, Describing uncertainties in single-sample experiments, Mechanical Engineering 75 (1953) 3–8.
[64] K.W. Bewig, W.A. Zisman, The wetting of gold and platinum by water, The Journal of Physical Chemistry 69 (12) (1965) 4238–4242.
[65] M.L. White, The wetting of gold surfaces by water, Journal of Physical Chemistry 68 (10) (1964) 3083–3085.

Please cite this article in press as: C.A. Hernández-Bocanegra et al., Measurement of heat flux in dense air-mist cooling: Part I – A novel steady-state technique, Exp. Therm. Fluid Sci. (2012), http://dx.doi.org/10.1016/j.expthermflusci.2012.06.015